



The research on the effect of dynamic tilt variation on the phase of cold atomic gravimeter

Peijun Chen^{1,2} · Yin Zhou¹ · Dong Zhu¹ · Kainan Wang¹ · Chan Zhang¹ · Shuping Peng¹ · Bing Cheng¹ · Bin Wu¹ · Qiang Lin¹

Received: 8 January 2024 / Accepted: 13 May 2024 / Published online: 4 June 2024
© The Author(s) 2024

Abstract

In recent years, absolute gravity comparison experiments between cold atomic gravimeter and traditional gravimeter have been carried out by combining cold atomic gravimeter with stable platform. Due to the working characteristics of the stable platform, the tilt angle of the cold atomic gravimeter will change slightly in the process of dynamic measurement, and the measurement noise will be introduced. In order to improve the accuracy of dynamic measurement, this paper first analyzes the trajectory of the mirror and atom in the atomic gravimeter combined with carrier motion information, obtains the phase expression of the atomic interferometer using the translation and rotation matrix, evaluates the main terms of the gravity deviation using the 20-min navigation data on the ship in the South China Sea, and simplifies the higher-order small-terms in the main terms to deduce the simplified form of the gravity deviation. Then, the Fourier transform is used to transform the simplified expression into the power spectrum expression of phase noise, the corresponding noise sensitivity function is used in the form of trigonometric. The 20-min data is divided into 10 intervals, the root-mean-square (RMS) value of the overall gravity deviation is 1.5–3 mGal using the power spectrum of the platform angle, angular velocity and carrier acceleration in each interval. The variation fluctuation of the RMS value is consistent with the fluctuation of solving the gravity deviation through the trajectory. The conclusion provides the calculation method of gravity noise caused by dynamic tilt change and horizontal acceleration, and also provides the basis for platform design.

1 Introduction

The cold atomic gravimeter (CAG) has the characteristics of high precision, high sensitivity and durable stability [1]. In recent years, with the rapid development of laser controlled atom technology [2, 3], people have moved the CAG out of the laboratory and carried out dynamic absolute gravity measurement comparison experiments on ship [4–6] and airborne [7, 8]. For example, Bidet conducted airborne tests on the French coast [8], comparing the CAG with the classical LaCoste & Romberg gravimeter and the new iMAR strap-down inertial measurement unit, the experimental results showed that the CAG was superior in measurement accuracy

and long-term stability. During dynamic measurement, the CAG is fixed on a stable platform [9], which is used to isolate the angular motion of the carrier. Researchers have used various methods to improve the accuracy of absolute gravity measurements. A novel method of the modulated Coriolis effect is proposed when the cold atom gravimeter was tested on the lake, since the cold atoms have horizontal velocity when they fall freely, and the phase difference caused by the Coriolis force needs to be compensated [5]. The data fusion of the atomic gravimeter and accelerometer is realized by the Kalman filter algorithm which observing the outputs of the atomic gravimeter and accelerometer, it can restrain the influence of dynamic vibration noise and obtain high precision gravity information in real time [6]. The method of the gravity estimation from the flying data is using the lowpass filtering which filtering the data of kinematic acceleration and the *Eötvös* effect, and correcting of the alignment errors of the platform, when the cold atom gravimeter is taken gravity measurements on airplanes [7]. These experimental results show that CAG can provide more accurate absolute

✉ Shuping Peng
pengshuping@zjut.edu.cn

¹ Zhejiang Provincial Key Laboratory of Quantum Precision Measurement, Zhejiang University of Technology, Hangzhou 310023, China

² School of mechanical and electrical engineering, Huangshan University, Huangshan 245041, China

gravity acceleration information for modern navigation, geophysics, resource exploration and other fields [10].

The high-precision CAG itself has multiple noise sources [11], the influences of Raman light intensity [12], two-photon light shift [14] and wavefront aberrations [14] have been analyzed. However, similar to the relative gravimeter, the CAG is also very sensitive to tilt in dynamic measurement process. For the strapdown inertial relative gravimeter, the product of the attitude matrix and the specific force vector is taken as an interference term of the gravity measurement and corrected, and for the relative gravimeter based on a stable platform, the cross-coupling error and platform tilt correction need to be corrected simultaneously [15]. Furthermore, for the cold atom gravimeters, researchers have studied less about the gravity measurement errors caused by attitude, the relevant conclusion is that the gravity deviation is proportional to the square value of the tilt angle under static conditions [16]. When the CAG are carried out under dynamic conditions, due to the influence of the external environment, the horizontal attitude of the stable platform is always in the adjustment process [17], so the tilt angle of the gravimeter is changed, there is additional relative motion between the mirror and the atom in the measurement process, coupled with the horizontal velocity and acceleration of the carrier. Therefore, the dynamic tilt change is regarded as a measurement noise that also causes gravity deviation. In order to improve the accuracy of gravity measurement, it is necessary to evaluate the effect of changing angle.

2 The dynamic measuring device and the noise from angle and angular velocity

2.1 Dynamic absolute gravity measuring device

The dynamic absolute gravity measuring device is a combination of the CAG and the stable platform, the schematic diagram of the dynamic measurement system is shown in Fig. 1. The CAG is fixed directly above the stable platform frame, the mirror is fixed on the upper surface of the accelerometer, and the accelerometer and strapdown inertial navigation system (INS) is fixed directly below the platform frame, the INS is under the accelerometer, where the distance between the mirror surface and the rotation center is l_0 .

The CAG is based on Mach-Zehnder interferometer [11], and the theoretical basis is two-photon Raman transition. The Raman light k_1 and k_2 reflected by the mirror form a pair of opposite Raman light beams. The interference process is summarized as follows: the ^{87}Rb cold atomic group is released from 3D-MOT center, and the atomic wave packet undergo the beam splitting, deflecting and merging by passing $\pi/2 - \pi - \pi/2$ three beams of the opposite Raman light.

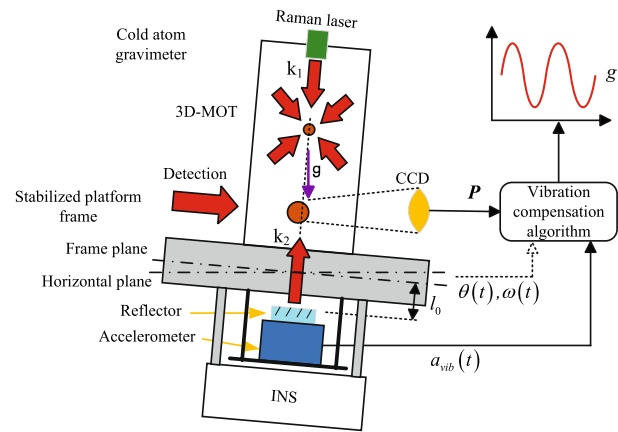


Fig. 1 The schematic diagram of measuring device based dynamic cold atom gravimeter

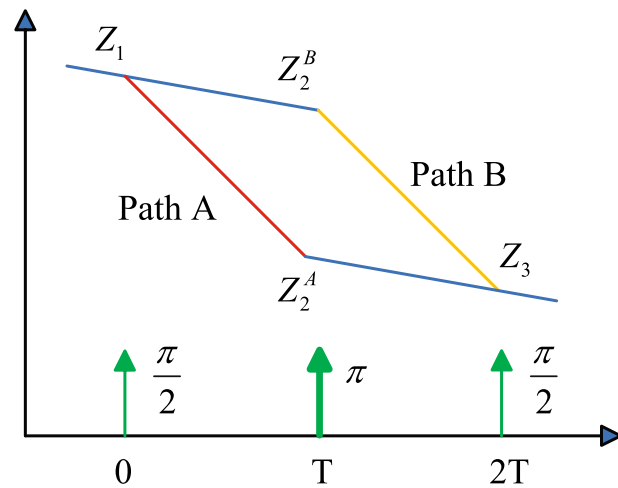


Fig. 2 Schematic diagram of three-pulse atomic interference path

Finally, the normalized atomic population P is obtained by detecting the fluorescence signal of the atoms. The expression P is as follows,

$$P = P_0 + C \cos(\Delta\Phi) \tag{1}$$

where P_0 and C are respectively the DC bias and amplitude of the atomic interference fringe, and $\Delta\Phi$ the interference phase-shift difference of the atomic wave packet. The atomic wave packet goes through two interference paths, A and B, before merging the beam, and the atoms in the two paths feel different laser phase-shifts[18], as shown in Fig. 2.

The phase-shift difference $\Delta\Phi$ between the two paths is shown as follows,

$$\begin{aligned} \Delta\Phi &= \Phi_A - \Phi_B = \Phi(z_1) - \Phi(z_2^A) - \Phi(z_2^B) + \Phi(z_3) \\ &= (\mathbf{k} \cdot \mathbf{g} - \alpha)T^2 + \Delta\Phi_{vib} \end{aligned} \tag{2}$$

where z_1, z_2^A, z_2^B, z_3 is the coordinate value of atom in light field, \mathbf{k} is the effective wave vector of Raman light, g is the local acceleration of gravity, α is the chirp rate of Raman light frequency, T is the pulse interval, $\Delta\Phi_{vib}$ is the vibration phase. It contains the information of the local absolute gravity value, and also contains the noise of phase-shift change of the light field from the vibration of mirror. Therefore, vibration compensation algorithm must be added to obtain accurate absolute gravity value from measurement data. In the dynamic measurement process, the mirror and atomic wave packets are moving on the earth's surface, and there is a relative motion between the mirror and the atoms, which increases the difficulty of analysis.

2.2 The noise of angle and angular velocity from stabilized platform

The platform is composed of a horizontal two-axis frame, namely a pitch axis and a roll axis. However, the measuring device is always affected by the external interference torque, and according to the control characteristics of the control system, the frame plane is always in the adjustment state, and the roll angle and pitch angle change within the allowed small range. For example, the attitude accuracy of the platform is 0.1 mrad in dynamic absolute gravity test conducted on ship [4] and airborne [7], the authors give the formula for calculating the gravity deviation caused by the tilt which estimated by combining the accelerometer data with GNSS data, and give the maximum value of the tilt deviation. Che Hao carried out absolute gravity measurement experiments on Qiandao Lake in Hangzhou [19], and the range of roll angle is 0.176 mrad, and the range of pitch angle is 0.035 mrad. Zhu Dong conducted an offshore absolute gravity test in the South China Sea [20], the paper pointed out that the real-time random rotation of the platform would also introduce measurement noise. The attitude data of the 20-min voyage for analysis is selected as shown in Fig. 3.

The values of attitude angle and angular velocity are derived from the data of INS in the stabilized platform. High precision F120HC fiber optic gyro is selected as the attitude sensor to obtain accurate tilt values, the accuracy of the horizontal attitude provided by INS is 4.85×10^{-5} rad, the accuracy of the heading angle is 8.7×10^{-4} rad. The geographic horizontal angle of the inertial stabilized platform is calculated from the information of fiber optic gyroscope, accelerometer and satellite positioning. The size of the heading angle will affect the accuracy of the geographic horizontal plane solution, and thus affect the precision of the horizontal attitude control.

As can be seen from the figure, the attitude has changed slowly with the change of heading angle which defined as the angle of north to east, also quickly complete the adjustment response in order to suppress the interference torque during

navigation in the South China Sea. The change amplitude of roll angle and pitch angle is 0.06 mrad and 0.05 mrad. Through the analysis of angular velocity power spectrum in Fig. 3d, it can be seen that the main frequency of the angular velocity change is around 10 Hz, the peak value at 10 Hz is $-80 \text{ (rad/s)}^2/\text{Hz}$, the result is 0.1 mrad/s.

The cold atom gravimeter is an absolute gravity measuring device based on the principle of mass-wave interference of cold atoms. The cold atoms feel the phase of Raman light in the process of falling, and its phase depends on the relative motion track of cold atoms in the light field. The Raman lasers are Gaussian beams, the change of heading angle does not affect the relative motion of cold atoms in the light field, but the horizontal attitude angle affects the coordinate axis of the Raman light field, so the relative motion track of cold atoms changes, and the phase also changes. The magnitude of the heading angle needs to be considered when compensating the Coriolis force effect, because the projection of horizontal velocity in the east–west direction will produce Coriolis force effect, and the projection in the north–south direction will not produce Coriolis force effect.

3 The formula of phase-shift difference under dynamic measurement

This section assumes that the absolute gravity value is g_{std} , the value of gravity deviation g_{bias} can be calculated by integrating the data of navigation and platform into the phase calculation, the expression g_{bias} is as follows,

$$g_{bias} = \frac{\Delta\Phi(x, y, z)}{kT^2} - g_{std} \quad (3)$$

then the main factors affecting gravity deviation can be evaluated, and the calculation formula of gravity noise can be obtained to simplify the evaluation method. Since the position of the atom in the Raman light field determines the phase of the atom, it is necessary to determine the phase-shift equation of the light field first.

3.1 The phase-shift equation of Raman light field

As can be seen from Fig. 1, the light field consists of a pair of Gaussian beams facing each other [21, 22]. Although the beam waist is not on the reflector, in order to facilitate the analysis of the phase size of the atom in the Raman light, we assume the limit case, that is, the beam waist of the Raman light is on the reflector, and evaluate the magnitude of the phase contribution of each item in the Gaussian formula. The phase equation of Gaussian beams in literature [23] is adopted, and the center of the reflecting mirror is selected as the origin, the phase-shift expression of the two Gaussian beams is shown in Formula 4 and 5, and the total phase shift

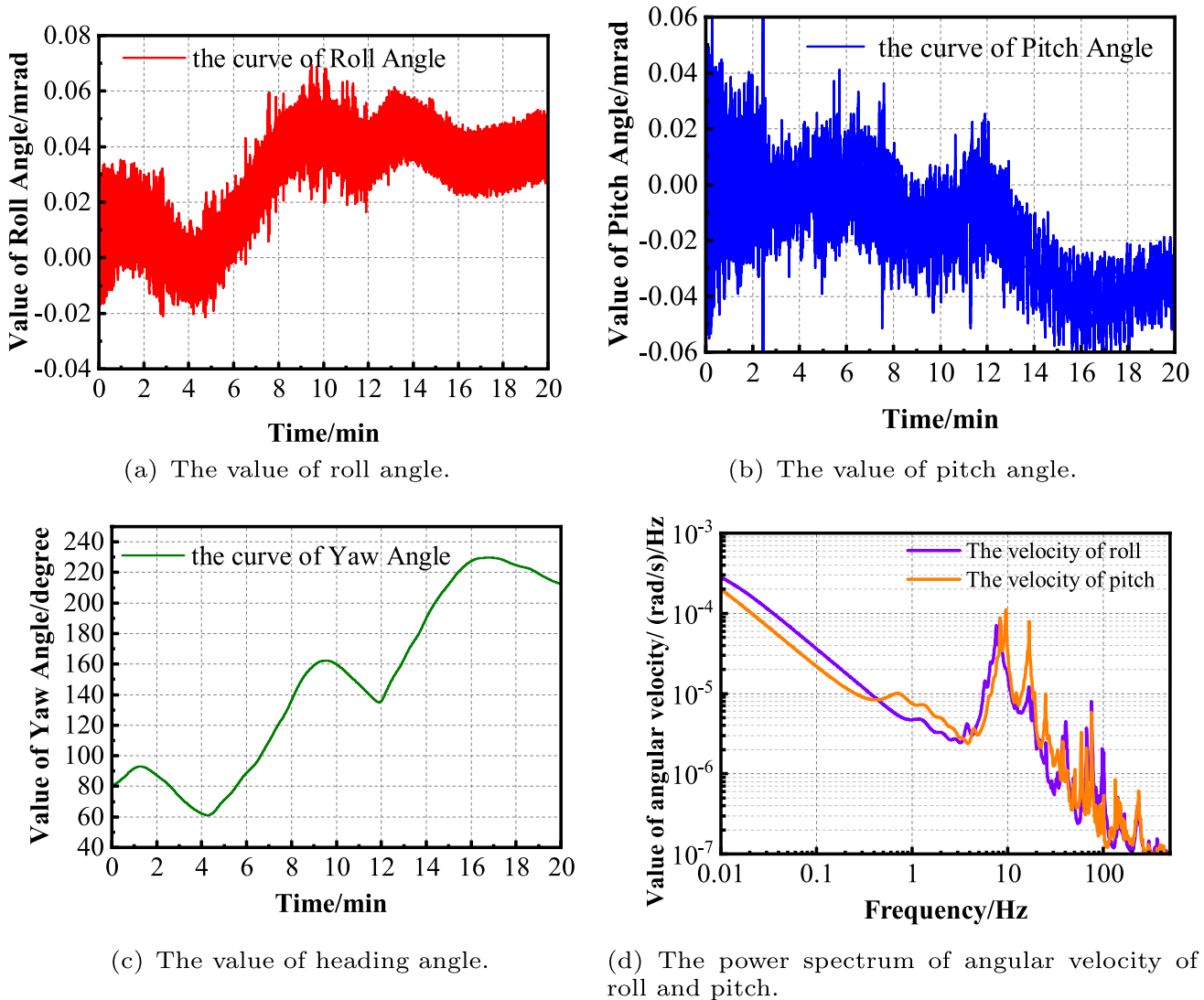


Fig. 3 The attitude data of platform in 20-min sailing

expression of light field is shown in Formula 6 after linear addition. It can be seen that the relative motion of the atom wave packet in the light field produces a phase difference,

$$\Phi_{k_1}(x, y, z) = k_1 z + k_1 \frac{(x^2 + y^2)}{2R(z)} - \arctan\left(\frac{z}{z_R}\right). \quad (4)$$

$$\Phi_{k_2}(x, y, -z) = - \left(-k_2(-z) + k_2 \frac{(x^2 + y^2)}{2R(-z)} - \arctan\left(\frac{-z}{z_R}\right) \right). \quad (5)$$

$$\begin{aligned} \Delta\Phi(x, y, z) &= \Phi_{k_1} + \Phi_{k_2} \\ &= k z + k \frac{(x^2 + y^2)}{2R(z)} - 2\arctan\left(\frac{z}{z_R}\right). \end{aligned} \quad (6)$$

where x, y, z is the three-dimensional coordinate value of the light field space, $k = k_1 - k_2$ is the effective wave vector of Raman light, $R(z) = z(1 + (z_R/z)^2)$ is the curvature radius of a Gaussian beam, $z_R = \pi\omega_0^2/\lambda$ is the Rayleigh distance, ω_0 is the waist of a Gaussian beam. In the experiment, we changed the Rayleigh distance by adjusting the lens group in the collimator, which was generally much larger than 50 m. In order to evaluate the phase deviation value generated by the curvature radius in the formula, we assumed that the Rayleigh distance was 50 m, that is, the second and third terms in the formula were increased. The phase expression

of light field Formula 6 contains three terms, namely, the linear phase of light field, the curvature phase of light field and the Gouy phase of light field.

3.2 Analysis of motion trajectories of atoms and light fields

3.2.1 Coordinate system selection

From the above formulas, it can be seen that the phase-shift difference is related to the coordinates of the atoms in light field, we use the geocentric inertial coordinate system $x^i y^i z^i$, the navigation coordinate system $x^n y^n z^n$ and the carrier coordinate system $x^b y^b z^b$ to analyze the trajectory of the two, as shown in Fig. 4.

As can be seen from the figure, the released atoms are subjected to the gravitational force F_G of the Earth, the centripetal force F_{ce} of the rotation around the center of the Earth, and the recoil F_{re} of the light which is related to the angle of the platform, the acceleration g is the component of the gravitational force. The z^n is coincident with g , the axis of Raman optical is coincident with z^b of the carrier. The function of stable platform is to isolate the angular motion of the carrier, so that z^b should overlaps z^n , in this way, the axis of Raman optical can be kept coincident with the gravitational vertical line. That is, the frame plane follows the horizontal plane of the local navigation system in Fig. 1.

Both the atom and the mirror are moving in the inertial coordinate system in Fig. 4, and the coordinate position of the atom in the light field determines the phase obtained by the atom. In order to solve the motion trajectory of the two, it is better to analysis in the stationary reference system, so we choose the geocentric inertial coordinate system (ECI) $x^i y^i z^i$, which does not rotate with the Earth. In the previous section, the center point of the reflecting mirror was taken as the origin point of the light field, and the mirror was fixed on the platform, so the carrier coordinate system $x^b y^b z^b$ was

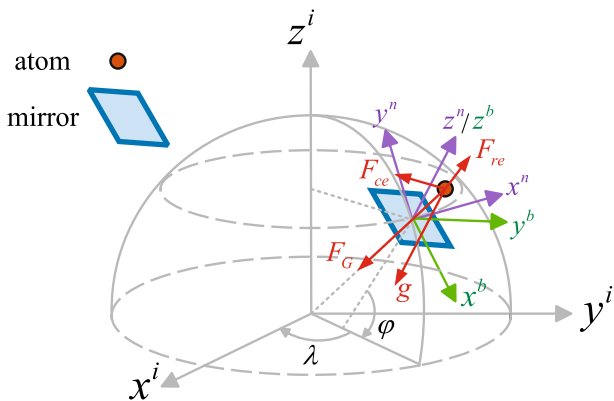


Fig. 4 The diagram of coordinate system and atomic force

chosen as the coordinate system of the light field, so that the light field would move and swing along with the platform, as shown in Fig. 5, and the counterclockwise rotation was positive.

In Fig. 5, θ and α is the attitude angle, the moment of atomic interference is $t_0, t_0 + T$ and $t_0 + 2T$, the position vector $S_{at}(t)$ of the atom and the position vector $S_{mi}(t)$ of the mirror moving with the platform are in the static reference frame, this can get the position vector $S_\phi(t) = S_{at}(t) - S_{mi}(t)$ of the atom in light field. The coordinate system of light field is rotated in a small angle with the platform, we can obtain the coordinate value of the position vector $S_\phi(t)$ in the light field using the rotation matrix $R(t)$, and then bring the coordinate value into the Formula 6, the total phase-shift difference $\Delta\phi(x, y, z)$ of the atom can be calculated, finally the gravity deviation value can be obtained. In the next section, the expression of the position vector is solved separately.

3.2.2 The motion equation of atom and mirror

In the dynamic measurement process, the atom has the same velocity as the carrier before release, the velocity is $v_0(t)$. After release, the atom and the carrier are affected by different accelerations. The acceleration of the atom is $a_{at}(t)$, the acceleration of the mirror which is the same as that of the carrier is $a_m(t)$. The following is the analysis of the motion trajectory, the calculation and derivation process is divided into 4 steps:

Step 1: Analyze trajectory of the atom. In the ECI coordinate system, the atoms are imprisoned in the 3D-MOT center before falling, the initial position vector of the atomic released is S_{ini} , the vector is composed of three parts, r_1, r_2, r_3 , and the three vectors are connected in turn. The starting point of r_1 is in the center of the Earth, and the end point of r_3 is in the center of the cold atom, where the size of r_1 is the radius of the Earth, the size of r_2 is the height from the platform to the horizontal plane, and the

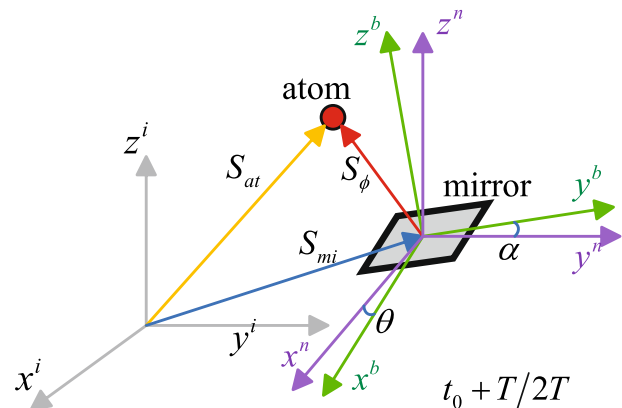


Fig. 5 The diagram of the vector relationship between an atom and a mirror

size of r_3 is the distance from the 3D-MOT to the mirror. When the atoms are in free fall, they are subjected to the gravitational force and the recoil of the light field, and it is difficult to analyze in the ECI coordinate system, we can calculate the trajectory of the motion by projecting the resultant force of the atoms into the navigation coordinate system.

On the one hand, atoms have angular velocity following the rotation of the Earth, so the force balance formula of atoms in a rotating reference system with constant angular velocity is as follows,

$$G \frac{Mm}{S_{ini}^2} = m \vec{\omega}_{ie} \times (\vec{\omega}_{ie} \times S_{ini} + \mathbf{v}_0(t)) + m \frac{d}{dt} (\vec{\omega}_{ie} \times S_{ini} + \mathbf{v}_0(t)) \tag{7}$$

where G is the gravitational constant, M is the mass of the Earth, m is the mass of the atom, ω_{ie} is the angular speed of the Earth's rotation, S_{ini} is the position vector of the cold atom, \times is the cross product symbol. The expression is as follows after removing parentheses and merging items of the same kind,

$$G \frac{Mm}{S_{ini}^2} + m\omega_{ie}^2 S_{ini} \cos\varphi - 2m \vec{\omega}_{ie} \times \mathbf{v}_0(t) = m \mathbf{a}_{at}(t) \tag{8}$$

where $G \frac{Mm}{S_{ini}^2} + m\omega_{ie}^2 S_{ini} \cos\varphi = mg$, $m\omega_{ie}^2 S_{ini} \cos\varphi$ is the inertial centrifugal force, φ is the latitude, the gravity is the resultant force of gravitational force and centripetal force, $2m \vec{\omega}_{ie} \times \mathbf{v}_0$ is the Coriolis force. The dynamic equation of the atom is as follows,

$$mg - 2m \vec{\omega}_{ie} \times \mathbf{v}_0(t) = m \mathbf{a}_{at}(t) \tag{9}$$

the resultant force of atom is affected by the velocity $\mathbf{v}_0(t)$ of carrier in the navigation coordinate system. Assumption that the initial time t_0 is 0, the trajectories of atoms is

$$S'_{at}(t) = S_{ini} + \int_0^t \mathbf{v}_0(t) dt + \int_0^t \int_0^t \mathbf{a}_{at}(t) dt dt \tag{10}$$

On the other hand, the Raman light has a recoil on the atom, and the displacement is related to the current tilt angle which is the angle between the carrier coordinate system and the navigation coordinate system, so the corresponding displacement vector $S_{recoil}(t)$ is as follows,

$$S_{recoil}(t) \approx \frac{k\hbar T}{m} \begin{pmatrix} -\theta(t) \\ \alpha(t) \\ 1 - (\theta(t)^2 + \alpha(t)^2)/2 \end{pmatrix} \tag{11}$$

since the roll angle and pitch angle are generally small, the value of \sin or \cos can be simplified to the angle value $\sin\theta(t) = \theta(t)$, $\cos\theta(t) = 1 - \theta(t)^2/2$.

Then the displacement vector expression for path A and path B is as follows:

$$\begin{aligned} S_{at}^A(0) &= S_{ini} \\ S_{at}^A(T) &= S_{ini} + S'_{at}(T) + S_{recoil}(T) \\ S_{at}^B(T) &= S_{ini} + S'_{at}(T) \\ S_{at}^B(2T) &= S_{ini} + S'_{at}(2T) + S_{recoil}(T) \end{aligned} \tag{12}$$

Step 2: Analyze trajectory of the mirror. It can be seen from the structure of Fig. 1, the mirror and the classical accelerometer are fixed together, the specific force value which is the output of the accelerometer acts as the resultant force of the mirrors. Because of the tilt angle, the acceleration vector of the mirror is projected into the navigation coordinate system, the expression $\mathbf{a}_m(t)$ is as follows,

$$\mathbf{a}_m(t) = \begin{pmatrix} a'_{mx}(t) \\ a'_{my}(t) \\ a'_{mz}(t) \end{pmatrix} = \begin{pmatrix} a_{mx}^*(t)(1 - \frac{\alpha(t)^2}{2}) - a_{mz}^*(t)\alpha(t) \\ a_{my}^*(t)(1 - \frac{\theta(t)^2}{2}) + a_{mz}^*(t)\theta(t) \\ a_{mz}^*(t)(1 - \frac{\alpha(t)^2}{2} - \frac{\theta(t)^2}{2}) - a_{mx}^*(t)\alpha(t) + a_{my}^*(t)\theta(t) \end{pmatrix} \tag{13}$$

where a_{mx}^* , a_{my}^* , a_{mz}^* is the specific force output value of the accelerometer, a'_{mx} , a'_{my} , a'_{mz} is the projection vector of the specific force value in the navigation coordinate system. The displacement vector of the mirror is calculated as follows,

$$\begin{aligned} S_m(0) &= S_{ini} - S_0 \\ S_m(T) &= S_{ini} - S_0 + \int_0^T \int_0^T \mathbf{a}_m(t) dt dt \\ S_m(2T) &= S_{ini} - S_0 + \int_0^{2T} \int_0^{2T} \mathbf{a}_m(t) dt dt \end{aligned} \tag{14}$$

Step 3: Analyze rotation matrix. Since the center of the mirror is not the center of rotation, the distance between the mirror and the rotation center is l_0 , firstly the coordinate origin is moved to the rotation center, and then the rotation matrix in the carrier coordinate system is obtained by using the attitude angle, finally the rotating coordinate origin is moved back to the reflecting mirror, the final rotation matrix is $R(t) = D(l_0)T(\alpha_t)T(\theta_t)D(-l_0)$

$$R(t) = \begin{pmatrix} 1 - \frac{\theta_t^2}{2} & \alpha_t \theta_t & \alpha_t (1 - \frac{\theta_t^2}{2}) & \alpha_t (1 - \frac{\theta_t^2}{2}) l_0 \\ 0 & 1 - \frac{\theta_t^2}{2} & -\theta_t & \theta_t l_0 \\ -\alpha_t & \theta_t (1 - \frac{\theta_t^2}{2}) & (1 - \frac{\theta_t^2}{2})(1 - \frac{\alpha_t^2}{2}) & l_0 (1 - (1 - \frac{\theta_t^2}{2})(1 - \frac{\alpha_t^2}{2})) \\ 0 & 0 & 0 & 1 \end{pmatrix} \tag{15}$$

Step 4: The expression of total phase-shift. After calculating the position vector and rotation matrix, we can calculate the coordinate value of the atom at each moment in the light field, the expression is as follows,

$$\begin{pmatrix} z_1 \\ 1 \end{pmatrix} = R(0) \begin{pmatrix} S_{at}^A(0) - S_m(0) \\ 1 \end{pmatrix} \quad \begin{pmatrix} z_2^A \\ 1 \end{pmatrix} = R(T) \begin{pmatrix} S_{at}^A(T) - S_m(T) \\ 1 \end{pmatrix} \\
 \begin{pmatrix} z_2^B \\ 1 \end{pmatrix} = R(T) \begin{pmatrix} S_{at}^B(T) - S_m(T) \\ 1 \end{pmatrix} \quad \begin{pmatrix} z_3 \\ 1 \end{pmatrix} = R(2T) \begin{pmatrix} S_{at}^B(2T) - S_m(2T) \\ 1 \end{pmatrix} \tag{16}$$

finally, combined with Formula 2, the total phase shift difference is calculated.

At present, researchers will use the data of vertical acceleration to compensate vibration phase compensation both static and dynamic, so vertical acceleration $a_z^* = 0$ is not considered here. The Coriolis force effect is caused by the speed of the ship over a long period of time [5], so this bias is also eliminated in the final data processing. Therefore, in the process of solving the single atomic interference, the attitude angle data of the platform and the horizontal acceleration data of the platform are only selected.

4 Data analysis and simulation

4.1 Shipboard data results

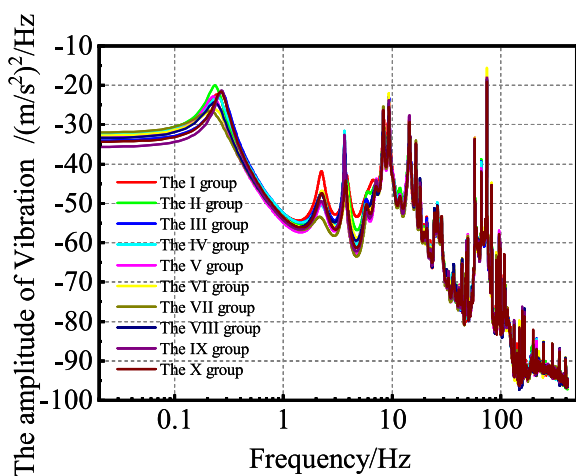
In order to evaluate the influence of each item in Formula 6 to the gravity deviation, this paper uses 20-min data of the ship-borne from Sect. 2 into the above Formula 10, 11, 12, 13, 14, 15, 16, where the tilt value of the platform is selected from Fig. 4. The sampling frequency of the accelerometer is 2kHz, which leads to a large amount of vibration data, so the 20-min data of vibration is divided into 10 intervals for convenient to analyze, as the duration of 120 s is enough to calculate the spectrum density down to 0.01 Hz range. The

power spectrum curves of each interval are drawn together for comparison in Fig. 6.

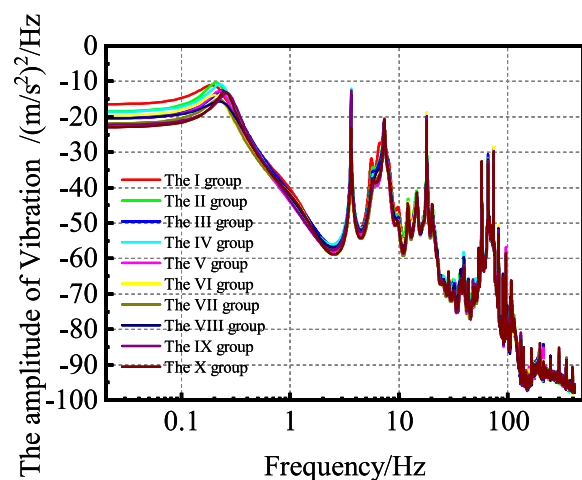
It can be seen from Fig. 6 that the vibration amplitude in the Y-axis direction is slightly larger than that in the X-axis direction. There is a peak value 0.1 m/s² in the X-axis and 0.3 m/s² in the Y-axis both at 0.2Hz, which is caused by waves hitting the hull. When the frequency is less than 0.2Hz, both X-axis and Y-axis have DC components, indicating that the ship is moving horizontally. Around the frequencies of 10 Hz and 80 Hz, a large number of high-frequency vibrations appear, and these vibrations become the main source of external interference.

The calculation results of each item in Formula 6 are shown in Fig. 7, where Fig. 7a is the gravity deviation value generated by the linear phase of the light field, and Fig. 7b is the gravity deviation value generated by the radius of curvature. As can be seen from the figure, the gravity deviation mainly comes from the linear phase of the light field as the peak-to-peak is less than 8 mGal, the peak-to-peak value of deviation caused by the curvature is less than 0.007 mGal, moreover the deviation caused by the Gouy phase is less than 2×10^{-5} mGal, which is not plotted, is ignored in subsequent calculations.

The horizontal acceleration of the carrier causes the cold atom to deviate from the central axis of the Raman laser. As can be seen from the spatial geometric relationship, the gravity deviation value generated by the curvature radius is symmetric with the central axis and decreases along the radius. The gravity deviation generated by the curvature radius increases with the distance from the central axis, so the curve in Fig. 7b is always negative. It can be seen from Fig. 7a that the fluctuation of gravity deviation value is consistent with the fluctuation of tilt in Fig. 3a and b.

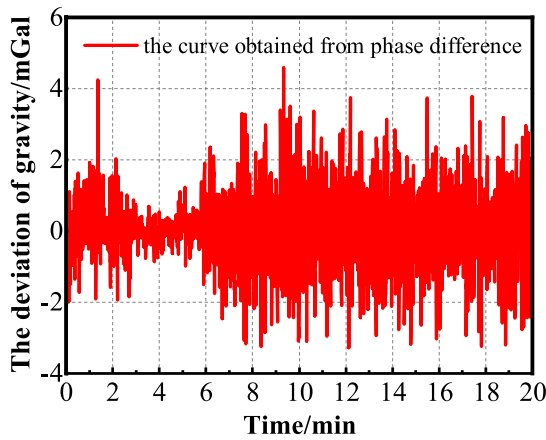


(a) Power spectrum amplitude in the X-axis direction.

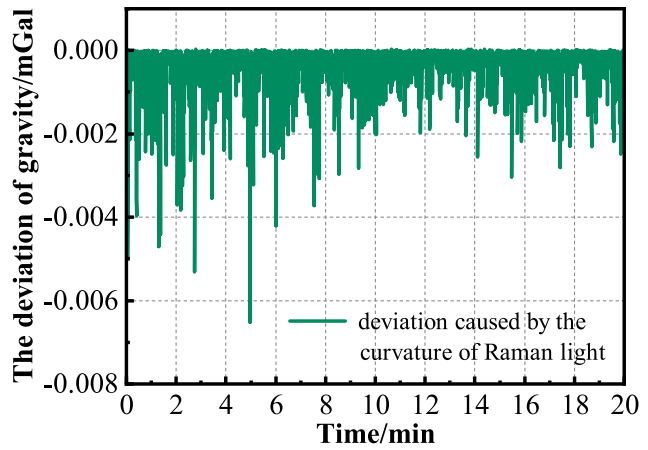


(b) Power spectrum amplitude in the Y-axis direction.

Fig. 6 Power spectrum analysis of 10 groups of carrier horizontal vibration



(a) Gravity deviation curve generated by linear phase.



(b) Gravity deviation curve generated by curvature phase.

Fig. 7 The calculated result of gravity deviation

4.2 Simplification of linear phase

The conclusion in the above section is that the main source of gravity deviation is the linear phase of the light field, but the calculation process is too complicated and is not conducive to engineering application, so the expression needs to be simplified. First, the third row of the rotation matrix is acted as the rotation vector $r(t)$ which is as follow,

$$r(t) = \begin{pmatrix} -\alpha_t \\ \theta_t(1 - \alpha_t^2/2) \\ (1 - \theta_t^2/2)(1 - \alpha_t^2/2) \\ l_0 - l_0(1 - \theta_t^2/2)(1 - \alpha_t^2/2) \end{pmatrix}^T \quad (17)$$

the linear phase of the light field in Formula 6 can be obtain by multiplying the rotation vector with the position vector, thus the analysis process is simplified. Second, the acceleration of the carrier and the attitude change of the platform are time-varying, it is difficult to analyze, so assuming that the π pulse time is zero moment, the atom and mirror velocity is \mathbf{v}_{at}^* and \mathbf{v}_m^* respectively at this time, the angular velocity ω_θ , ω_α is constant in $2T$ time. Since the acceleration sampling rate of the carrier is 2 kHz, the acceleration of the carrier is chosen as the average acceleration \mathbf{a}_{m_1} , \mathbf{a}_{m_2} during the T time of atomic fall, as shown in Fig. 8.

Considering that the distance caused by the recoil of Raman light is small, it can be omitted, that is $S_{recoil}(t) = 0$. Then, at the time of three Raman pulses, the position vector expression of the atom in path A and path B can be transformed as follows.

$$\begin{aligned} *z_1 &= r(0)((S_{at}(T) - S_m(T)) - (\mathbf{v}_{at} - \mathbf{v}_M) + (\mathbf{g} - \mathbf{a}_{m_1})T^2/2) \\ *z_2^A &= r(T)(S_{at}(T) - S_m(T)) \\ *z_2^B &= r(T)(S_{at}(T) - S_m(T)) \\ *z_3 &= r(2T)((S_{at}(T) - S_m(T)) - (\mathbf{v}_{at} + \mathbf{v}_M) + (\mathbf{g} - \mathbf{a}_{m_2})T^2/2) \end{aligned} \quad (18)$$

where $*z_2^A = *z_2^B = *z_2$. Then the Formula 2 can be simplified as follows,

$$\Delta\Phi = \Phi_A - \Phi_B = \Phi(*z_1) - 2\Phi(*z_2) + \Phi(*z_3) \quad (19)$$

the position vector of Formula 18 is multiplied by the rotation vector of Formula 17, the result is then brought into Formula 19 to obtain the phase calculation expression which is as follows,

$$\Delta\Phi_z = \begin{pmatrix} (k'_0 - 2k'_T + k'_{2T})(S_{at}(T) - S_m(T)) - (k'_0 - k'_{2T})(\mathbf{v}_{at} - \mathbf{v}_M)T \\ +(k'_0 + k'_{2T})\mathbf{g}T^2 - (k'_0\mathbf{a}_{m_1} + k'_{2T}\mathbf{a}_{m_2})T^2/2 + \Delta\Phi_{l_0} \end{pmatrix} \quad (20)$$

where $k'_i = \mathbf{k}(-\alpha_i, \theta_i, 1 - \theta_i^2/2 - \alpha_i^2/2)^T$, $\Delta\Phi_{l_0}$ is the phase deviation caused by the distance of the Raman mirror from the center of rotation. The deviation of the linear phase can

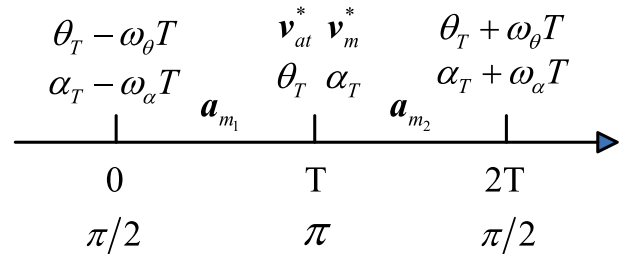


Fig. 8 The relationship diagram of tilt angle, angular velocity, acceleration and interference time

be simplified as two terms, the tilt term $\Delta\Phi_{tilt}$ and the angular velocity term $\Delta\Phi_{\omega}$ by omitting the higher-order terms of Formula 20. The detailed derivation process is in Appendix A. The expression is as follows,

$$\Delta\Phi_{tilt} \approx -k(-2\alpha_T \bar{a}_{m_x}^* + 2\theta_T \bar{a}_{m_y}^*)T^2 \tag{21}$$

$$\Delta\Phi_{\omega} \approx -k(-\bar{a}_{m_x}^* \int_{-T}^T \omega_{\alpha} dt + \bar{a}_{m_y}^* \int_{-T}^T \omega_{\theta} dt)T^2. \tag{22}$$

The expression of tilt term $\Delta\Phi_{tilt}$ is slightly different from the expression of gravity deviation caused by tilt in literature [7], which is reflected in two aspects. The first is that the X-axis direction is a negative sign, which is related to the choice of the carrier coordinate system; the second is that the product result of horizontal acceleration and angle is two times, because both the accelerometer vector and the rotating light field vector contain horizontal attitude information, the horizontal acceleration vector is shown in Formula (13), and the light field vector is shown in Formula (17). When the two vectors are multiplied and higher-order minor terms are ignored, the scale factor 2 appears.

The angular velocity term $\Delta\Phi_{\omega}$ is the product of the integral of angular velocity and the horizontal acceleration. We have assumed that the angular velocity ω_{α} and ω_{θ} is unchanging in $2T$ time period, so it can be simplified as follows,

$$\Delta\Phi_{\omega} \approx -k(-2\omega_{\alpha} \bar{a}_{m_x}^* + 2\omega_{\theta} \bar{a}_{m_y}^*)T^3 \tag{23}$$

the deviation of the final gravity value is expressed as follows,

$$-\Delta g = -\frac{\Delta\Phi_{\omega} + \Delta\Phi_{tilt}}{kT^2} \approx (-2\alpha_T \bar{a}_{m_x}^* + 2\theta_T \bar{a}_{m_y}^*) + (-2\omega_{\alpha} \bar{a}_{m_x}^* + 2\omega_{\theta} \bar{a}_{m_y}^*)T. \tag{24}$$

4.3 Phase noise expression of dynamic angle

The premise of the derivation of the above formula is that the time sequence of the atom falling and the stable platform can be synchronized, but the attitude and horizontal acceleration data of the platform at present do not match the time point of the atom falling, so it cannot be used for phase compensation. The dynamic angle change and the carrier acceleration are taken as the measurement noise, and the root-mean-square value of gravity noise caused by dynamic angle change can be solved by combining with the corresponding sensitivity function.

First, we calculate the power spectral of the relevant data series of inertial navigation output, Fourier transform is applied to Formula 24 to obtain the power spectral $S_g(\omega)^2$

of gravity noise caused by dynamic angle change, as shown in the following expression,

$$S_g(\omega)^2 = \frac{4F_x(\omega) * G_x(\omega)}{4\pi^2} + \frac{4F_y(\omega) * G_y(\omega)}{4\pi^2} + \frac{4F_x(\omega) * U_x(\omega)T^2}{4\pi^2} + \frac{4F_y(\omega) * U_y(\omega)T^2}{4\pi^2}. \tag{25}$$

where $*$ is a convolution symbol, $F_x(\omega)$ and $F_y(\omega)$ is power spectrum of horizontal vibration, $G_x(\omega)$ and $G_y(\omega)$ is power spectrum of platform attitude angle, $U_x(\omega)$ and $U_y(\omega)$ is power spectrum of platform attitude angular velocity.

The 20-min data of in Sect. 4.1 is divided into 10 intervals, each interval is 2 min, and the corresponding gravity noise power spectral curve was obtained by using Formula 25, as shown in Fig. 9.

Second, a noise sensitivity function $h(t)$ is needed to solve the phase[24]. Since the cold atom interference process can be regarded as a $2T$ time sampling process on the time sequence, the function is in the form of Trigonometric form[25], the time-domain expression is as follows,

$$h(t) = \begin{cases} 1/T + t/T^2 & -T \leq t \leq 0 \\ 1/T - t/T^2 & 0 < t \leq T \end{cases} \tag{26}$$

the corresponding Fourier transform is $H(\omega)$, the expression is as follows,

$$H(\omega) = \frac{2 - e^{iT\omega} - e^{-iT\omega}}{T^2\omega^2}. \tag{27}$$

the curve of the transfer function is shown in the Fig. 10, when the T is 20 ms, it can be seen that the transfer function has low-pass filtering characteristics, and the cutoff frequency is 10 Hz.

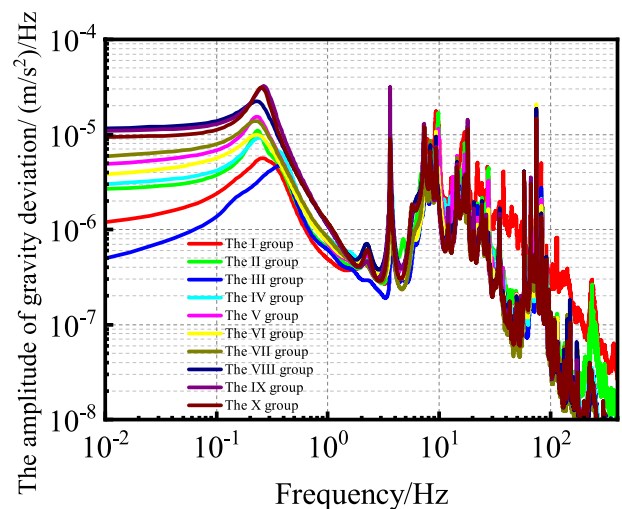


Fig. 9 The curve of gravity noise power spectral

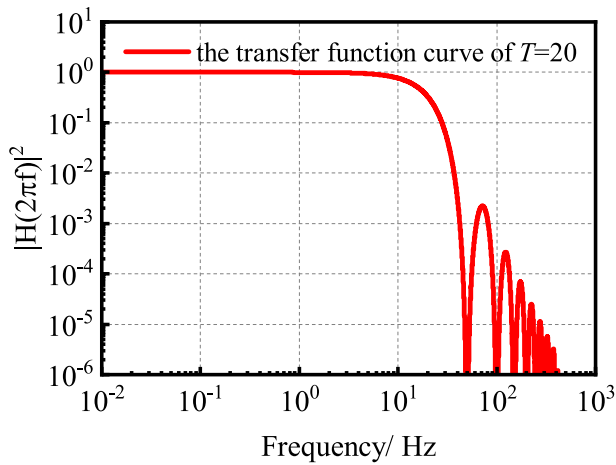


Fig. 10 Transfer function curve of triangle function

Finally, the root-mean-square value σ_g^{rms} of gravity noise is calculated by integrating the sensitivity function $H(\omega)$ and the noise power spectral $S_g(\omega)$, and the expression is as follows[24].

$$(\sigma_g^{rms})^2 = \int_0^\infty |H(\omega)|^2 S_g(\omega) d\omega. \tag{28}$$

The root-mean-square value of gravity noise in each interval is obtained by using the results from Fig. 9, and the calculation results of Formula 28 is compared with those of Fig. 7a, as shown in Fig. 11. The blue diamond in the figure is the root-mean-square value of gravity noise from the perspective of frequency domain, while the red curve is the real-time value of gravity deviation calculated from the perspective of time domain, the calculation results of the two methods can accurately reflect the deviation of gravity value caused by the dynamic tilt angle, and are basically consistent.

In the actual dynamic absolute gravity measurement process, we can obtain the power spectral of the platform's horizontal vibration, attitude angle and angular velocity, the root-mean-square value of gravity noise caused by the dynamic angle change can be evaluated by using Formula 28. It can see from Fig. 11, the deviation of measurement results is caused by the change of platform attitude angle, which is mainly caused by the displacement of the Raman light mirror relative to the atom. However, the result of multiplying the horizontal acceleration with the attitude angle and angular velocity of the stable platform is a linear part in the total displacement of the mirror.

Although this 1.5–3 mGal noise level is smaller than the typical noise level after vertical motion vibration compensation, it is not the main noise to be considered at present, the measurement accuracy will be further improved through further studying the synchronization of the platform and atomic

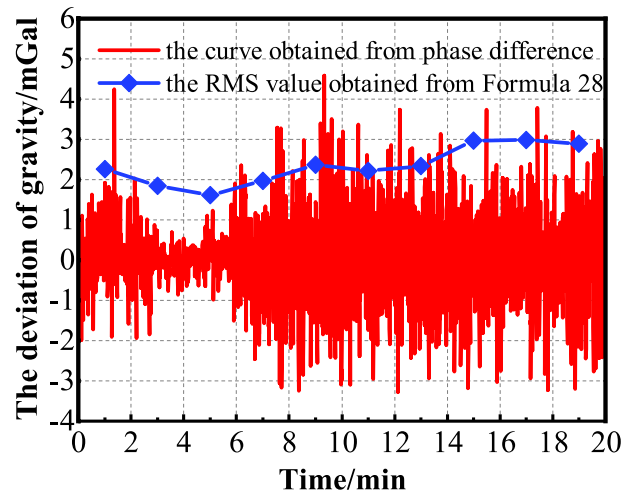


Fig. 11 Transfer function curve of triangle function

gravimeter to verify the effect of noise suppression in the future. Besides, the result can also provides a basis for the control accuracy design of the stable platform.

The control task of the stable platform is to maintain the gravimeter at the local geographic level, and the attitude control accuracy is related to the attitude solution algorithm of INS and the parameters of the sensor in the stable platform. In the 20-min sailing data used in this paper, the attitude control accuracy of the stable platform will change with the change of the azimuth angle when the carrier is moving, and the simulation results show that the gravity measurement results are biased. In the process of dynamic measurement, the atomic gravimeter itself is not sensitive to the azimuth angle, but the attitude control accuracy of the stable platform is related to the azimuth angle, resulting in the gravity measurement deviation. If the round-trip measurement method is adopted on the measurement line, the mean value of the horizontal attitude is zero, which avoids the problem of gravity measurement deviation.

5 Summary

In this paper, the attitude change of the stable platform is analyzed by using the sailing data of the absolute gravity measurement carried out by the cold atom gravimeter in the South China Sea, the angular velocity is concentrated in 0.1 mrad/s, and the peak of the horizontal acceleration of the carrier is 0.1 m/s² and 0.3 m/s². In order to improve the measurement accuracy of absolute gravity value, this paper deduces the phase calculation expression of atoms in the rotating light field, and estimates that the phase deviation mainly comes from the linear phase by combining with the

actual sailing data. Then, by simplifying the linear phase expression, the simplest phase deviation expression including the tilt term and the angular velocity term is obtained, and the corresponding noise sensitivity function $S_g(\omega)$ is obtained by using the simplest expression, the transfer function $H(\omega)$ in the form of trigonometric is used. The RMS value curve of gravity noise is obtained by combining the power spectrum of attitude, angular velocity and horizontal acceleration, the range of the value is 1.5–3 mGal, and the variation fluctuation is consistent with the result of trajectory phase method. This method can be used to evaluate the gravity noise generated by the dynamic angle change of the platform, and improve the accuracy of the dynamic absolute gravity measurement, furthermore it provides a basis for the control accuracy index of the platform design.

Currently, the cold atom gravimeter and the stable platform work independently, however the timing of the two can be synchronized by communication method, it can provides a design idea for a new dynamic compensation algorithm based on the angle and angular velocity of the atom interference moment. In the future, the two can be further integrated, the cold atomic gravimeter can provide local absolute gravity information for the stable platform, correct the influence of zero drift of the sensor, and further improve the control accuracy of the platform.

Derivation of formula

Formula 20 has the following form:

$$\Delta\Phi_z = \begin{pmatrix} (k'_0 - 2k'_T + k'_{2T})(S_{at}(T) - S_m(T)) - (k'_0 - k'_{2T})(v_{at} - v_m)T \\ + (k'_0 + k'_{2T})gT^2 - (k'_0 a_{m_1} + k'_{2T} a_{m_2})T^2/2 + \Delta\Phi_{i_0} \end{pmatrix}. \quad (29)$$

where $k'_t = \mathbf{k}(-\alpha_t, \theta_t, 1 - \theta_t^2/2 - \alpha_t^2/2)^T$. The expression contains a total of five items. Let's break it down:

The first item: $(k'_0 - 2k'_T + k'_{2T})(S_{at}(T) - S_m(T))$,

$$(k'_0 - 2k'_T + k'_{2T}) = \mathbf{k} \begin{pmatrix} -\int_{-T}^T f(t)\omega_\alpha(t)dt \\ \int_{-T}^T f(t)\omega_\theta(t)dt \\ -\sigma_1 \end{pmatrix}^T, \quad (30)$$

$$f(t) = \begin{cases} +1 & -T \leq t \leq 0 \\ -1 & 0 \leq t \leq T \end{cases}$$

where $\sigma_1 = (\alpha_0^2/2 + \theta_0^2/2 + \alpha_{2T}^2/2 + \theta_{2T}^2/2 - \alpha_T^2 + \theta_T^2) = (\omega_\alpha^2 + \omega_\theta^2)T^2$, in one interference period, assuming angular velocity is constant, then $\int_{-T}^T \omega_\alpha(t)dt = 0$, $\int_{-T}^T \omega_\theta(t)dt = 0$.

From the data analysis in Sect. 2.2, it can be seen that the magnitude of angular amplitude and angular velocity is in mrad, and both of them are high-order minor terms after squared. Then the first term is simplified as follows:

$$(k'_0 - 2k'_T + k'_{2T})(S_{at}(T) - S_m(T)) \approx -k\sigma_1 l_1 \approx -kl_1(\omega_\alpha^2 + \omega_\theta^2)T^2 \approx 0 \quad (31)$$

where l_1 is the length of the Z-axis component between the atom and the mirror at the time of π .

The second item: $-(k'_0 - k'_{2T})(v_{at}^* - v_m^*)T$,

$$k'_0 - k'_{2T} = \mathbf{k} \begin{pmatrix} \int_{-T}^T \omega_\alpha(t)dt \\ -\int_{-T}^T \omega_\theta(t)dt \\ -\theta_0^2/2 - \alpha_0^2/2 + \theta_{2T}^2/2 + \alpha_{2T}^2/2 \end{pmatrix}^T \quad (32)$$

where $-\theta_0^2/2 - \alpha_0^2/2 + \theta_{2T}^2/2 + \alpha_{2T}^2/2 \approx 0$. We know that the initial velocity of the atom and the mirror is the same, $v_{at}^* - v_m^*$ is the relative velocity difference which depends on the acceleration difference $\mathbf{g} - \mathbf{a}_{m_1}$ between the atom and the mirror at the time of π . Since the acceleration of the mirror does not drastically change during atom fall, in order to analyze the influence of the acceleration in an interference process, the expression of the relative velocity difference becomes $v_{at}^* - v_m^* \approx (\mathbf{g} - (\mathbf{a}_{m_1} + \mathbf{a}_{m_2})/2)$.

The vector expression for gravity and acceleration which as follows is plugged into the second term,

$$\mathbf{g} = \begin{pmatrix} 0 \\ 0 \\ -g \end{pmatrix},$$

$$\mathbf{a}_{m_1} = \begin{pmatrix} \bar{a}'_{m_{1x}} \\ \bar{a}'_{m_{1y}} \\ \bar{a}'_{m_{1z}} \end{pmatrix} = \begin{pmatrix} \bar{a}^*_{m_{1x}}(1 - \alpha_0^2/2) - \bar{a}^*_{m_{1z}}\alpha_0 \\ \bar{a}^*_{m_{1y}}(1 - \theta_0^2/2) + \bar{a}^*_{m_{1z}}\theta_0 \\ \bar{a}^*_{m_{1z}}(1 - \alpha_0^2/2 - \theta_0^2/2) - \bar{a}^*_{m_{1x}}\alpha_0 + \bar{a}^*_{m_{1y}}\theta_0 \end{pmatrix},$$

$$\mathbf{a}_{m_2} = \begin{pmatrix} \bar{a}'_{m_{2x}} \\ \bar{a}'_{m_{2y}} \\ \bar{a}'_{m_{2z}} \end{pmatrix} = \begin{pmatrix} \bar{a}^*_{m_{2x}}(1 - \alpha_T^2/2) - \bar{a}^*_{m_{2z}}\alpha_T \\ \bar{a}^*_{m_{2y}}(1 - \theta_T^2/2) + \bar{a}^*_{m_{2z}}\theta_T \\ \bar{a}^*_{m_{2z}}(1 - \alpha_T^2/2 - \theta_T^2/2) - \bar{a}^*_{m_{2x}}\alpha_T + \bar{a}^*_{m_{2y}}\theta_T \end{pmatrix}. \quad (33)$$

where $\mathbf{a}_{m_1}, \mathbf{a}_{m_2}$ is the mean value from Fig. 8, compare with the Formula 13, $\bar{a}^*_{m_{1x}}, \bar{a}^*_{m_{1y}}, \bar{a}^*_{m_{1z}}$ is the mean of the three axes of the accelerometer in the first period T , $\bar{a}^*_{m_{2x}}, \bar{a}^*_{m_{2y}}, \bar{a}^*_{m_{2z}}$ is the mean of the three axes of the accelerometer in the second period T , $\bar{a}'_{m_{1x}}, \bar{a}'_{m_{1y}}, \bar{a}'_{m_{1z}}, \bar{a}'_{m_{2x}}, \bar{a}'_{m_{2y}}, \bar{a}'_{m_{2z}}$ is the projection of the acceleration value on the navigation axis. After multiplying and omitting the higher order terms, the vector expression is as follows,

$$-(k'_0 - k'_{2T})(v_{at}^* - v_m^*)T \approx -\mathbf{k}T^2 \begin{pmatrix} -\int_{-T}^T \omega_\alpha(t)dt((\bar{a}^*_{m_{1x}} + \bar{a}^*_{m_{2x}})/2 + (\bar{a}^*_{m_{1z}}\alpha_0 + \bar{a}^*_{m_{2z}}\alpha_T)/2) \\ +\int_{-T}^T \omega_\theta(t)dt((\bar{a}^*_{m_{1y}} + \bar{a}^*_{m_{2y}})/2 + (\bar{a}^*_{m_{1z}}\theta_0 + \bar{a}^*_{m_{2z}}\theta_T)/2) \end{pmatrix}. \quad (34)$$

where $\int_{-T}^T \omega_\alpha(t)dt(\bar{a}^*_{m_{1z}}\alpha_0 + \bar{a}^*_{m_{2z}}\alpha_T)/2 \approx 0$, $\int_{-T}^T \omega_\theta(t)dt(\bar{a}^*_{m_{1z}}\theta_0 + \bar{a}^*_{m_{2z}}\theta_T)/2 \approx 0$, because the result of the product of the acceleration value and the square of angle value can also be regarded as a higher order minor term. And you end up with,

$$-(k'_0 - k'_{2T})(v_{at}^* - v_m^*)T \approx -kT^2 \left(-\int_{-T}^T \omega_\alpha(t)dt \bar{a}_{m_x}^* + \int_{-T}^T \omega_\theta(t)dt \bar{a}_{m_y}^* \right). \tag{35}$$

where $(\bar{a}_{m_{1x}}^* + \bar{a}_{m_{2x}}^*)/2 = \bar{a}_{m_x}^*$, $(\bar{a}_{m_{1y}}^* + \bar{a}_{m_{2y}}^*)/2 = \bar{a}_{m_y}^*$ are the average acceleration. The above results are defined as $\Delta\Phi_\omega$, it is the product of the angular change and the horizontal acceleration of the accelerometer during atom interference.

The third item: $(k'_0 + k'_{2T})gT^2/2$

$$(k'_0 + k'_{2T})/2 = k \begin{pmatrix} -\alpha_0 - 0.5 \int_{-T}^T f(t)\omega_\alpha(t)dt \\ \theta_0 + 0.5 \int_{-T}^T f(t)\omega_\theta(t)dt \\ 1 - \theta_0^2/4 - \alpha_0^2/4 - \theta_{2T}^2/4 - \alpha_{2T}^2/4 \end{pmatrix}^T. \tag{36}$$

Since the gravity vector is $\mathbf{g} = \begin{pmatrix} 0 \\ 0 \\ -g \end{pmatrix}$, the result is as follows after multiplying and omitting higher order terms.

$$(k'_0 + k'_{2T})gT^2/2 = -k\mathbf{g}T^2 (1 - \theta_0^2/4 - \alpha_0^2/4 - \theta_{2T}^2/4 - \alpha_{2T}^2/4) \approx -k\mathbf{g}T^2 \tag{37}$$

The fourth item: $-(k'_0 \mathbf{a}_{m_1} + k'_{2T} \mathbf{a}_{m_2})T^2/2$, substitute the acceleration vector into the fourth term, and the expressions are as follows.

$$k'_0 \mathbf{a}_{m_1} = k \begin{pmatrix} -\alpha_0 \\ \theta_0 \\ 1 - \alpha_0^2/2 - \theta_0^2/2 \end{pmatrix}^T \begin{pmatrix} \bar{a}_{m_{1x}}^* (1 - \alpha_0^2/2) - \bar{a}_{m_{1z}}^* \alpha_0 \\ \bar{a}_{m_{1y}}^* (1 - \theta_0^2/2) + \bar{a}_{m_{1z}}^* \theta_0 \\ \bar{a}_{m_{1z}}^* (1 - \alpha_0^2/2 - \theta_0^2/2) - \bar{a}_{m_{1x}}^* \alpha_0 + \bar{a}_{m_{1y}}^* \theta_0 \end{pmatrix} \approx k(-2\alpha_0 \bar{a}_{m_{1x}}^* + 2\theta_0 \bar{a}_{m_{1y}}^* - \bar{a}_{m_{1z}}^*) \tag{38}$$

$$k'_{2T} \mathbf{a}_{m_2} = k \begin{pmatrix} -\alpha_{2T} \\ \theta_{2T} \\ 1 - \alpha_{2T}^2/2 - \theta_{2T}^2/2 \end{pmatrix}^T \begin{pmatrix} \bar{a}_{m_{2x}}^* (1 - \alpha_{2T}^2/2) - \bar{a}_{m_{2z}}^* \alpha_{2T} \\ \bar{a}_{m_{2y}}^* (1 - \theta_{2T}^2/2) + \bar{a}_{m_{2z}}^* \theta_{2T} \\ \bar{a}_{m_{2z}}^* (1 - \alpha_{2T}^2/2 - \theta_{2T}^2/2) - \bar{a}_{m_{2x}}^* \alpha_{2T} + \bar{a}_{m_{2y}}^* \theta_{2T} \end{pmatrix} \approx k(-2\alpha_{2T} \bar{a}_{m_{2x}}^* + 2\theta_{2T} \bar{a}_{m_{2y}}^* - \bar{a}_{m_{2z}}^*) \tag{39}$$

The angle values of the above expression are unified into α_T , θ_T , it is able to get

$$-(k'_0 \mathbf{a}_{m_1} + k'_{2T} \mathbf{a}_{m_2})T^2/2 \approx \begin{pmatrix} -k(-\alpha_T(\bar{a}_{m_{1x}}^* + \bar{a}_{m_{2x}}^*) + \theta_T(\bar{a}_{m_{1y}}^* + \bar{a}_{m_{2y}}^*)) + (\bar{a}_{m_{1z}}^* + \bar{a}_{m_{2z}}^*)/2 \\ -\omega_\theta T(\bar{a}_{m_{1y}}^* - \bar{a}_{m_{2y}}^*) - \omega_\alpha T(\bar{a}_{m_{1x}}^* - \bar{a}_{m_{2x}}^*) \end{pmatrix} T^2 \tag{40}$$

where $-\omega_\theta T(\bar{a}_{m_{1y}}^* - \bar{a}_{m_{2y}}^*) - \omega_\alpha T(\bar{a}_{m_{1x}}^* - \bar{a}_{m_{2x}}^*)T^2 \approx 0$ is the product of the change in acceleration value and the angular velocity, and it is considered that the higher order small

term, $(\bar{a}_{m_{1x}}^* + \bar{a}_{m_{2x}}^*)/2 = \bar{a}_{m_x}^*$, $(\bar{a}_{m_{1y}}^* + \bar{a}_{m_{2y}}^*)/2 = \bar{a}_{m_y}^*$, $(\bar{a}_{m_{1z}}^* + \bar{a}_{m_{2z}}^*)/2 = \bar{a}_{m_z}^*$, the resulting expression is as follows,

$$-(k'_0 \mathbf{a}_{m_1} + k'_{2T} \mathbf{a}_{m_2})T^2/2 \approx -kT^2(-2\alpha_T \bar{a}_{m_x}^* + 2\theta_T \bar{a}_{m_y}^* + \bar{a}_{m_z}^*) \tag{41}$$

In the time domain calculation method of vertical vibration compensation, trigonometric function is used to multiply the vertical vibration value. Since the result of expression $(\bar{a}_{m_{1z}}^* + \bar{a}_{m_{2z}}^*)/2 = \bar{a}_{m_z}^*$, is the same as the result of trigonometric function in vibration compensation algorithm, $kT^2 \bar{a}_{m_z}^*$ is equivalent to the vibration compensation algorithm in the vertical direction. Define the remaining two terms as $\Delta\Phi_{tilt}$, it is the phase deviation produced by the tilt angle of Raman light and the horizontal acceleration, and the expression is as follows,

$$-(k'_0 \mathbf{a}_{m_1} + k'_{2T} \mathbf{a}_{m_2})T^2/2 \approx -kT^2(-2\alpha_T \bar{a}_{m_x}^* + 2\theta_T \bar{a}_{m_y}^*) \tag{42}$$

The fifth item: $\Delta\Phi_{l_0}$ is the phase deviation caused by the deviation of the Raman light mirror from the length of the rotation center, since there is a square of the angular velocity, this is a higher order term,

$$\Delta\Phi_{l_0} = kl_0 \sigma_1 = kl_0(\omega_\theta + \omega_\alpha)T^2 \approx 0. \tag{43}$$

Acknowledgements This work was supported in part by National Natural Science Foundation of China, Study on cold atom interference airborne dynamic absolute gravity measurement in non-uniform gravity field (U2341246), Research and application experiment of carrying measurement and support technology for ocean route (DD20191004), Research on active vibration isolation technology of cold atom gravimeter based on magnetic suspension inertial stabilized platform (51905482), Systematic error study of cold atom gravimeter in joint phase operation mode (11704334).

Author contributions P.C. wrote the main manuscript text. Y.Z. shared the research ideas and analysis methods. D.Z. provided the South China Sea navigation data and analyzed it together. K.W. and C.Z. shared the research idea of optical equation. S.P. shared the platform's control

strategy. C.B. guides the ideas of the article, puts forward opinions and guides the author to revise, and B.W. and Q.L. offered guiding advice. All authors reviewed the manuscript.

Data availability The data that support the findings of this study are available on request from the first author. The email address is 105093@hsu.edu.cn. The author can provide the calculation formulas involved in the paper, which are generally matlab scripts.

Declarations

Conflict of interest The authors declare no competing interests.

Open Access This article is licensed under a Creative Commons Attribution 4.0 International License, which permits use, sharing, adaptation, distribution and reproduction in any medium or format, as long as you give appropriate credit to the original author(s) and the source, provide a link to the Creative Commons licence, and indicate if changes were made. The images or other third party material in this article are included in the article's Creative Commons licence, unless indicated otherwise in a credit line to the material. If material is not included in the article's Creative Commons licence and your intended use is not permitted by statutory regulation or exceeds the permitted use, you will need to obtain permission directly from the copyright holder. To view a copy of this licence, visit <http://creativecommons.org/licenses/by/4.0/>.

References

- G. Rosi, F. Sorrentino, L. Cacciapuoti, M. Prevedelli, G.M. Tino, Precision measurement of the Newtonian gravitational constant using cold atoms. *Nature* **510**(7506), 518–521 (2014). <https://doi.org/10.1038/nature13433>
- C.S. Adams, E. Riis, Laser cooling and trapping of neutral atoms. *Prog. Quantum Electron.* **21**(1), 1–79 (1997). [https://doi.org/10.1016/S0079-6727\(96\)00006-7](https://doi.org/10.1016/S0079-6727(96)00006-7)
- O. Carraz, F. Lienhart, R. Charrière, M. Cadoret, N. Zahzam, Y. Bidel, A. Bresson, Compact and robust laser system for onboard atom interferometry. *Appl. Phys. B* **97**(2), 405–411 (2009). <https://doi.org/10.1007/s00340-009-3675-9>
- Y. Bidel, N. Zahzam, C. Blanchard, A. Bonnin, M. Cadoret, A. Bresson, D. Rouxel, M.F. Lequentrec-Lalancette, Absolute marine gravimetry with matter-wave interferometry. *Nat. Commun.* **9**(1), 627 (2018). <https://doi.org/10.1038/s41467-018-03040-2>
- Y. Zhou, C. Zhang, P.J. Chen, B. Cheng, D. Zhu, K.A. Wang, X.L. Wang, B. Wu, Z.K. Qiao, Q. Lin, R. Li, A testing method for shipborne atomic gravimeter based on the modulated coriolis effect. *Sensors* (2023). <https://doi.org/10.3390/s23020881>
- C.-F. Huang, A. Li, F.-J. Qin, J. Fang, X. Chen, An atomic gravimeter dynamic measurement method based on kalman filter. *Meas. Sci. Technol.* **34**(1), 015013 (2023). <https://doi.org/10.1088/1361-6501/ac8e8b>
- Y. Bidel, N. Zahzam, A. Bresson, C. Blanchard, M. Cadoret, A. Olesen, R. Forsberg, Absolute airborne gravimetry with a cold atom sensor. *J. Geodesy* (2020). <https://doi.org/10.1007/s00190-020-01350-2>
- Y. Bidel, N. Zahzam, A. Bresson, C. Blanchard, A. Bonnin, J. Bernard, M. Cadoret, T.E. Jensen, R. Forsberg, C. Salaun, S. Lucas, M.F. Lequentrec-Lalancette, D. Rouxel, G. Gabalda, L. Seoane, D.T. Vu, S. Bruinsma, S. Bonvalot, Airborne absolute gravimetry with a quantum sensor, comparison with classical technologies. *J. Geophys. Res. Solid Earth* **128**(4), 2022–025921 (2023). <https://doi.org/10.1029/2022JB025921>
- J.M. Hillert, Inertially stabilized platform technology concepts and principles. *IEEE Control Syst. Mag.* **28**(1), 26–46 (2008). <https://doi.org/10.1109/MCS.2007.910256>
- B. Fang, I. Dutta, P. Gillot, D. Savoie, J. Lautier, B. Cheng, C. Alzar, R. Geiger, S. Merlet, F. Santos, A. Landragin, Metrology with atom interferometry: inertial sensors from laboratory to field applications. *J. Phys. Conf. Ser.* (2016). <https://doi.org/10.1088/1742-6596/723/1/012049>
- M. Kasevich, S. Chu, Measurement of the gravitational acceleration of an atom with a light-pulse atom interferometer. *Appl. Phys. B* **54**(5), 321–332 (1992). <https://doi.org/10.1007/BF00325375>
- Q.Q. Hu, H. Zhou, Y.K. Luo, Q. Luo, W.J. Kuang, F.B. Wan, Y.Y. Zhong, F.F. Xu, Improving the fringe contrast in an atomic gravimeter by optimizing the Raman laser intensity. *Optik* (2023). <https://doi.org/10.1016/j.ijleo.2023.170637>
- A. Gauguier, T.E. Mehlstaubler, T. Leveque, J. Le Gouet, W. Chaibi, B. Canuel, A. Clairon, F.P. Dos Santos, A. Landragin, Off-resonant Raman transition impact in an atom interferometer. *Phys. Rev. A* (2008). <https://doi.org/10.1103/PhysRevA.78.043615>
- V. Schkolnik, B. Leykauf, M. Hauth, C. Freier, A. Peters, The effect of wavefront aberrations in atom interferometry. *Appl. Phys. B* **120**(2), 311–316 (2015). <https://doi.org/10.1007/s00340-015-6138-5>
- C.L. Glennie, K.P. Schwarz, A.M. Bruton, R. Forsberg, A.V. Olesen, K. Keller, A comparison of stable platform and strapdown airborne gravity. *J. Geodesy* **74**(5), 383–389 (2000). <https://doi.org/10.1007/s001900000082>
- B. Wu, B. Cheng, Z.-J. Fu, D. Zhu, Y. Zhou, K.-X. Weng, X.-L. Wang, Q. Lin, Measurement of absolute gravity based on cold atom gravimeter at large tilt angle. *Acta Phys. Sin.* **67**(19), 190302 (2018). <https://doi.org/10.7498/aps.67.20181121>
- M.K. M, Inertially stabilized platforms for optical imaging systems. *IEEE Control Syst. Mag.* **28**(1), 47–64 (2008). <https://doi.org/10.1109/MCS.2007.910201>
- A. Peters, K.Y. Chung, S. Chu, High-precision gravity measurements using atom interferometry. *Metrologia* **38**(1), 25 (2001). <https://doi.org/10.1088/0026-1394/38/1/4>
- H. Che, A. Li, J. Fang, G.-G. Ge, W. Gao, Y. Zhang, C. Liu, J.-N. Xu, L.-B. Chang, C.-F. Huang, W.-B. Gong, D.-Y. Li, X. Chen, F.-J. Qin, Ship-borne dynamic absolute gravity measurement based on cold atom gravimeter. *Acta Phys. Sin.* (2022). <https://doi.org/10.7498/aps.71.20220113>
- D. Zhu, H. Xu, Y. Zhou, B. Wu, B. Cheng, K.-N. Wang, P.-J. Chen, S.-T. Gao, K.-X. Weng, H.-L. Wang, S.-P. Peng, Z.-K. Qiao, X.-L. Wang, Q. Lin, Data processing of shipborne absolute gravity measurement based on extended kalman filter algorithm. *Acta Phys. Sin.* (2022). <https://doi.org/10.7498/aps.71.20220071>
- Z.Y. Wang, T. Chen, X.L. Wang, Z. Zhang, Y.F. Xu, Q.A. Lin, A precision analysis and determination of the technical requirements of an atom interferometer for gravity measurement. *Front. Phys. China* **4**(2), 174–178 (2009). <https://doi.org/10.1007/s11467-009-0017-7>
- A. Louchet-Chauvet, T. Farah, Q. Bodart, A. Clairon, A. Landragin, S. Merlet, F.P. Dos Santos, The influence of transverse motion within an atomic gravimeter. *New J. Phys.* (2011). <https://doi.org/10.1088/1367-2630/13/6/065025>
- J. Hu, X. Chen, J. Fang, L. Zhou, J. Zhong, J. Wang, M. Zhan, Analysis and suppression of wave-front-aberration phase noise in weak-equivalence-principle tests using dual-species atom interferometers. *Phys. Rev. A* **96**(2), 023618 (2017). <https://doi.org/10.1103/PhysRevA.96.023618.PRA>
- P. Cheinet, B. Canuel, F.P.D. Santos, A. Gauguier, F. Yver-Leduc, A. Landragin, Measurement of the sensitivity function in a time-domain atomic interferometer. *IEEE Trans. Instrum. Meas.* **57**(6), 1141–1148 (2008). <https://doi.org/10.1109/TIM.2007.915148>

25. R. Geiger, V. Ménot, G. Stern, N. Zahzam, P. Cheinet, B. Battelier, A. Villing, F. Moron, M. Lours, Y. Bidel, A. Bresson, A. Landragin, P. Bouyer, Detecting inertial effects with airborne matter-wave interferometry. *Nat. Commun.* (2011). <https://doi.org/10.1038/ncomms1479>

Publisher's Note Springer Nature remains neutral with regard to jurisdictional claims in published maps and institutional affiliations.